JACS
JOURNAL OF THE AMERICAN CHEMICAL SOCIETY

ARTICLE

pubs.acs.org/JACS

The Roles of Molecular Structure and Effective Optical Symmetry in Evolving Dipolar Chromophoric Building Blocks to Potent Octopolar Nonlinear Optical Chromophores

Tomoya Ishizuka,[†,‡] Louise E. Sinks,[†,§] Kai Song,[∥] Sheng-Ting Hung,[⊥] Animesh Nayak,[†,#] Koen Clays,[*,⊥] and Michael J. Therien[*,#]

[†]Department of Chemistry, University of Pennsylvania, 231 South 34th Street, Philadelphia, Pennsylvania 19104-6323, United States

[∥]Beijing National Laboratory for Molecular Sciences, Key Laboratory of Photochemistry, Institute of Chemistry, Chinese Academy of Sciences, Beijing 100190, China

[⊥]Department of Chemistry, University of Leuven, B-3001 Leuven, Belgium

[#]Department of Chemistry, French Family Science Center, 124 Science Drive, Duke University, Durham, North Carolina 27708-0346, United States

Supporting Information

ABSTRACT: A series of mono-, bis-, tris-, and tetrakis(porphinato)zinc(II) (PZn)-elaborated ruthenium(II) bis(terpyridine) (Ru) complexes have been synthesized in which an ethyne unit connects the macrocycle *meso* carbon atom to terpyridyl (tpy) 4-, 4′-, and 4″-positions. These supermolecular chromophores, based on the ruthenium(II) [5-(4′-ethynyl-(2,2′;6′,2″-terpyridinyl))-10,20-bis(2′,6′-bis(3,3-dimethyl-1-butyloxy) phenyl)porphinato]zinc(II)-(2,2′;6′,2″-terpyridine)$^{2+}$ bis-hexafluorophosphate (RuPZn) archetype, evince strong mixing of the PZn-based oscillator strength with ruthenium terpyridyl charge resonance bands. Potentiometric and linear absorption spectroscopic data indicate that for structures in which multiple PZn moieties are linked via ethynes to a $[Ru(tpy)_2]^{2+}$ core, little electronic coupling is manifest between PZn units, regardless of whether they are located on the same or opposite tpy ligand. Congruent with these experiments, pump−probe transient absorption studies suggest that the individual RuPZn fragments of these structures exhibit, at best, only modest excited-state electronic interactions that derive from factors other than the dipole−dipole interactions of these strong oscillators; this approximate independent character of the component RuPZn oscillators enables fabrication of nonlinear optical (NLO) multipoles with extraordinary hyperpolarizabilities.

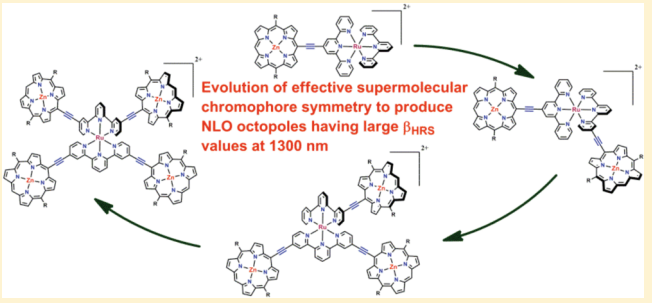

Dynamic hyperpolarizability (β_λ) values and depolarization ratios (ρ) were determined from hyper-Rayleigh light scattering (HRS) measurements carried out at an incident irradiation wavelength (λ_{inc}) of 1300 nm. The depolarization ratio data provide an experimental measure of chromophore optical symmetry; appropriate coupling of multiple charge-transfer oscillators produces structures having enormous averaged hyperpolarizabilities (β_{HRS} values), while evolving the effective chromophore symmetry from purely dipolar (e.g., Ru(tpy)[4-(Zn-porphyrin)ethynyl-tpy]$(PF_6)_2$, $\beta_{HRS} = 1280 \times 10^{-30}$ esu, $\rho = 3.8$; Ru(tpy)[4′-(Zn-porphyrin)ethynyl-tpy]$(PF_6)_2$, $\beta_{HRS} = 2100 \times 10^{-30}$ esu, $\rho = 3.8$) to octopolar (e.g., Ru[4,4″-bis(Zn-porphyrin)ethynyl-tpy]$_2(PF_6)_2$, $\beta_{HRS} = 1040 \times 10^{-30}$ esu, $\rho = 1.46$) via structural motifs that possess intermediate values of the depolarization ratio. The chromophore design roadmap provided herein gives rise to octopolar supermolecules that feature by far the largest off-diagonal octopolar first hyperpolarizability tensor components ever reported, with the effectively octopolar Ru[4,4″-bis(Zn-porphyrin)ethynyl-tpy]$_2(PF_6)_2$ possessing a β_{HRS} value at 1300 nm more than a factor of 3 larger than that determined for any chromophore having octopolar symmetry examined to date. Because NLO octopoles possess omnidirectional NLO responses while circumventing the electrostatic interactions that drive bulk-phase centrosymmetry for NLO dipoles at high chromophore concentrations, the advent of octopolar NLO chromophores having vastly superior β_{HRS} values at technologically important wavelengths will motivate new experimental approaches to achieve acentric order in both bulk-phase and thin film structures.

INTRODUCTION

Nonlinear optical (NLO) materials are used in a variety of applications, most notably in optical telecommunications, where NLO properties in the near-infrared (NIR) spectral region are used for frequency conversion and electro-optic modulation of signals. To engineer NLO chromophores, careful consideration

Received: June 8, 2010
Published: February 15, 2011

of molecular symmetry must be taken into account, as noncentrosymmetry is a prerequisite for all even-order, nonlinear effects.[1−10] The molecular properties that give rise to the NLO response are the electronic polarizability and the nature of the transitions between electronic states. Within the context of simple theoretical constructs, the experimental observables that are closely correlated with the magnitude of the molecular NLO response include (i) the frequency dependence of the ground-state molecular linear absorption spectrum, (ii) the absorption spectra of low-lying electronic states, and (iii) the oscillator strengths, transition energies, and changes in transition dipole moments associated with the transitions in these spectra.[11−18]

Insights derived from these theoretical frameworks have led to the development of organic and inorganic optoelectronic chromophores that manifest enhanced electronic hyperpolarizabilities (β_λ values). A classic molecular architecture that has been developed extensively has been the dipolar, donor−bridge−acceptor (D−Br−A) motif.[5−8,19−28] Numerous examples of dipolar D−Br−A chromophores that feature large dynamic hyperpolarizabilities exploit a highly polarizable porphyrinic component.[18,21−25,27−33] Along these lines, it has also been shown that strong conjugation mediated by an ethynyl unit between multiple porphyrinic components, or between porphyrin moieties and other strong oscillators, creates unusually polarizable and hyperpolarizable structures,[34−43] and has enabled the development of a variety of compositions and materials that possess unusual NLO properties.[44−54]

Porphyrin-based high β_λ chromophores that possess the most spectacular hyperpolarizabilities delineated to date feature (porphinato)zinc(II) (PZn) and metal(II)polypyridyl (M) units connected via an ethyne bridge. In these MPZn supermolecules, PZn $\pi-\pi^*$- and metal polypyridyl-based charge-resonance absorption oscillator strength are extensively mixed, and the respective charge transfer transition dipoles of these building blocks are aligned along the highly conjugated molecular axis. These structures manifest significant interpigment electronic interactions, display unusual dependences of the sign and magnitude of hyperpolarizability on incident irradiation frequency, and exhibit extraordinarily large β_λ values at telecommunications-relevant wavelengths.[18,25,29−31,45,47,48]

While large first hyperpolarizabilities have been realized for several dipolar, D−Br−A chromophores over the 1300−1500 nm spectral domain,[20,25,26,55,56] the development of macroscopic materials that possess impressive nonlinear properties based on these chromophores requires ordering of hyperpolarizable molecules in a non-centrosymmetric arrangement throughout the medium. For dipolar molecules, ground-state electrostatic interactions drive detrimental, centrosymmetric aggregation. Although experimental strategies exist that minimize the magnitude of antiparallel dipole−dipole interactions of NLO chromophores in the condensed phase, and facilitate electric-field poling of chromophoric guests in polymeric hosts to produce a processable materials for device fabrication, it is important to underscore that the net bulk-phase dipolar order realized in such NLO materials rarely, if ever, exceeds a level beyond that of several percent of the chromophoric dopants present in the medium.[9,56−62] Due in part to the ongoing challenge of obtaining uniform acentric order of dipolar NLO chromophores within a processable matrix, focus has been placed on the development of hyperpolarizable molecules having higher-order symmetry.

Multiple families of NLO chromophores having octopolar symmetry have been interrogated.[63−77] While such structures circumvent the electrostatic interactions that drive bulk-phase centrosymmetry at high chromophore concentrations, approaches other than electric-field-induced ordering, such as the synthesis of high generation dendritic octopoles,[71] spontaneous organization within an appropriate liquid-crystalline phase,[76] or all-optical poling,[78,79] need to be employed to organize NLO-active species of high-order symmetry. A challenge of equal importance lies in the fact that all NLO octopoles developed to date exhibit only modest responses at technologically important wavelengths relative to high β_λ dipolar chromophore benchmarks.

Evolution of NLO octopoles from dipolar chromophoric archetypes has been demonstrated, but such examples are confined largely to proof-of-principle targets that possess only modest hyperpolarizabilities; cases in point include the syntheses of 1,3,5-tridonor-2,4,6-triacceptor-aryl compounds inspired by the corresponding dipolar 1-donor-4-acceptor-aryl structures.[68,70,72−74,76] This fact has been emphasized recently by Torres and co-workers, who have noted that virtually all NLO octopoles reported to date are in fact octopolar expansions of the dipolar paradigm.[80] We show herein that ruthenium(II) [5-(4′-ethynyl-(2,2′;6′,2″-terpyridinyl))-10,20-bis(2′,6′-bis(3,3-dimethyl-1-butyloxy)phenyl)porphinato] zinc(II)-(2,2′;6′,2″-terpyridine)$^{2+}$ bis-hexafluorophosphate (RuPZn), a robust, benchmark dipolar chromophore that possesses an extraordinary β_λ value at a telecommunication-relevant wavelength ($\beta_{1300} = 5100 \times 10^{-30}$ esu),[25] can not only serve as a template for the development of an octopolar NLO chromophore (Figure 1); appropriate coupling of multiple, related charge-transfer oscillators can be utilized to evolve the effective chromophore optical symmetry in MPZn-based supermolecules from purely dipolar to octopolar, and generate octopolar NLO chromophores having impressive β_{HRS} values at 1300 nm.

EXPERIMENTAL SECTION

Materials. All manipulations were carried out under argon previously passed through an O_2 scrubbing tower (Schweizerhall R3-11 catalyst) and a drying tower (Linde 3 Å molecular sieves) unless otherwise stated. Air-sensitive solids were handled in a Braun 150-M glovebox. Standard Schlenk techniques were employed to manipulate air-sensitive solutions. All solvents utilized in this work were obtained from Fisher Scientific (HPLC grade). Tetrahydrofuran (THF) was distilled from Na/benzophenone under N_2. All NMR solvents and commercially available reagents were used as received unless noted otherwise. 2,2′-Dipyrrylmethane,[81,82] 4-bromo-(2,2′;6′,2″-terpyridine),[83] 4′-bromo-(2,2′;6′,2″-terpyridine),[83] 4,4″-dibromo-(2,2′;6′,2″-terpyridine),[83] and (2,2′;6′,2″-terpyridine)ruthenium(III) trichloride ($RuCl_3$(tpy)), along with its brominated derivatives,[84−88] were prepared by literature methods (see Supporting Information). Chemical shifts for ^{1}H NMR spectra are relative to the internal reference (tetramethylsilane) in $CDCl_3$, or solvent residual protium (acetonitrile-d_3, δ = 1.93 ppm). All J values are reported in Hertz. The number of attached protons is found in parentheses following the chemical shift value. Chromatographic purification (silica gel 60, 230−400 mesh, EM Scientific) of all newly synthesized compounds was accomplished on the benchtop. Standard abbreviations for metal polypyridyl compounds and terpyridyl are used throughout the Experimental Section.

Instrumentation. Electronic spectra were recorded on a Shimadzu UV-1700 spectrophotometry system. Cyclic voltammetric measurements were carried out on an EG&G Princeton Applied Research model

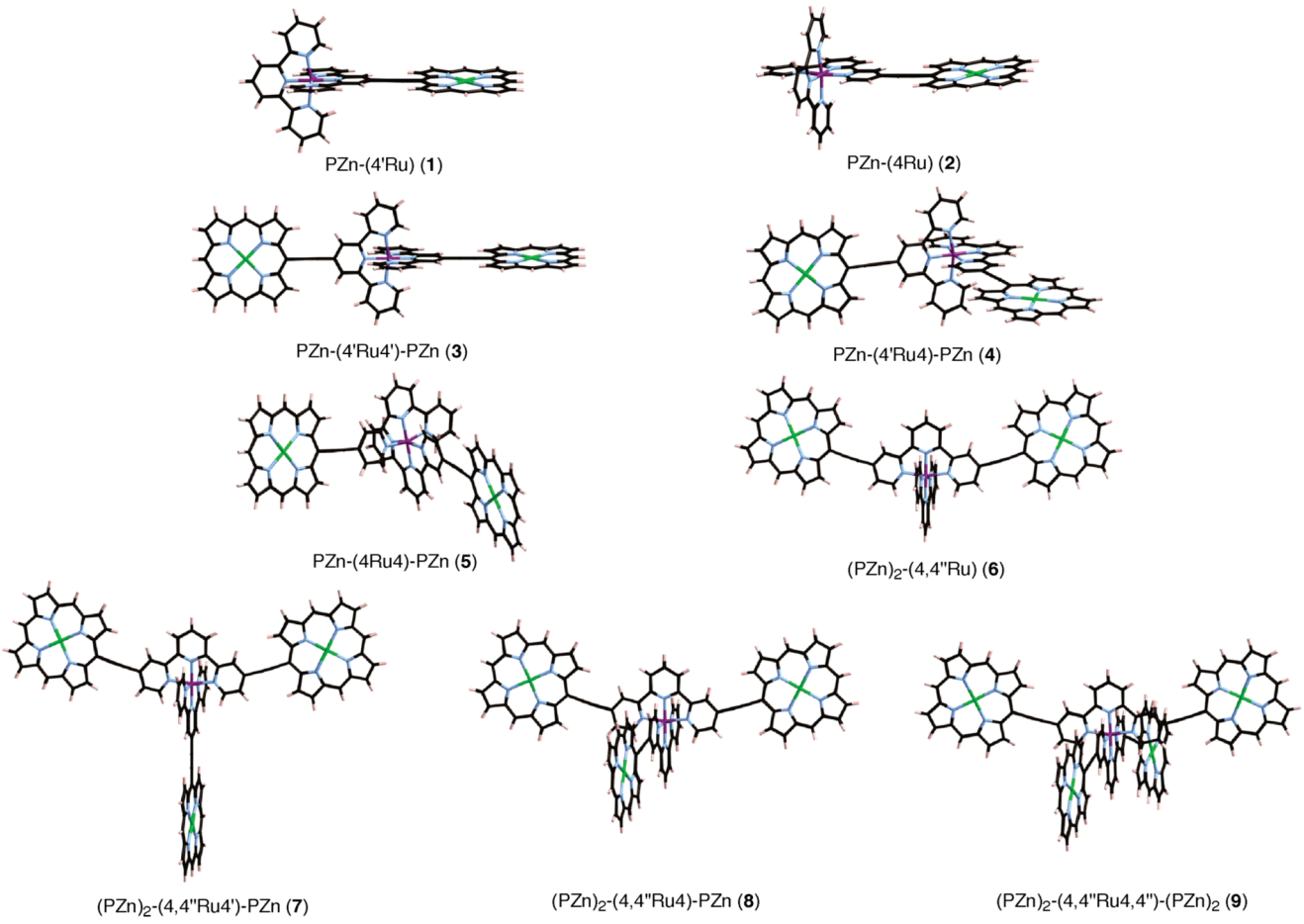

Figure 1. MM2-optimized structures of ethyne-bridged (porphinato)zinc(II)−ruthenium bis(terpyridine)-based chromophores **1**−**9**.

273A potentiostat/galvanostat. The electrochemical cell used for these experiments utilized a platinum disk working electrode, a platinum wire counter electrode, and a saturated calomel reference electrode (SCE). The reference electrode was separated from the bulk solution by a junction bridge filled with the corresponding solvent/supporting electrolyte solution. The ferrocene/ferrocenium redox couple was utilized as an internal potentiometric standard.

Ultrafast Transient Absorption Experiments. Transient absorption spectra were obtained using standard pump−probe methods. Optical pulses (>120 fs) centered at 775 nm were generated using a Ti:sapphire laser (Clark-MXR, CPA-2001), which consists of a regenerative amplifier seeded by a mode-locked fiber oscillator. A frequency-doubled near IR optical parametric amplifier (Clark-MXR) produced excitation pulses tunable throughout the visible region. The pump beam, chopped at half the laser repetition rate (∼500 Hz), was passed through an optical delay line. A fraction of the output from the regenerative amplifier was focused onto a 2 mm c-cut sapphire plate to generate a white light continuum, which was used as the probe beam. The polarization and attenuation of the pump and probe beams were controlled by a half-wave plate and Rochon prism polarizer pairs. The polarization was set to magic angle (54.7°) for these experiments. The pump beam was focused into the sample cell with an f = 40 cm lens, while the probe beam was focused with an f = 10 cm lens. After passing through the sample, the probe light was focused onto the entrance slit of the computer-controlled image spectrometer (SpectraPro-150, Acton Research Corporation). A CCD array detector (Roper Scientific, 1024 × 128 elements), interfaced to the spectrometer, recorded the spectrum of the probe light from the UV (∼370 nm) to the NIR (∼1100 nm), providing spectral resolution better than 0.5 nm. To provide shot-by-shot detection at a 1 kHz repetition rate, the entrance slit of the image spectrometer was optically masked to shield the upper bins of the CCD. Data points (32) were binned for each wavelength, with the resulting spectrum transferred to the computer. Pairs of consecutive spectra were measured with $I_{on}(\lambda)$ and $I_{off}(\lambda)$ to determine the difference spectrum, $\Delta A = \log(I_{off}(\lambda))/(I_{on}(\lambda))$. Transient spectra in 0.9−1.8 μm NIR region were recorded using a liquid-nitrogen-cooled InGaAs 512-element linear array detector (Roper Scientific) interfaced to a Spex-250 monochromator. All these experiments utilized a 2 mm path length fused-silica sample cell; all transient optical studies were carried out at 23 ± 1 °C. Samples were deoxygenated by three consecutive freeze−pump−thaw cycles prior to use. All transient spectra reported represent averages obtained over 4−6 scans, with each scan consisting of 100−170 time points.

The delay line utilized three computer-controlled delay stages. Short time delays were effected with Nanomover stages (Melles Griot), while longer delay times (up to 8.5 ns) were achieved using a Compumotor-6000 (Parker). The baseline noise level in these transient absorption experiments corresponded to ∼0.1 mOD per second of signal accumulation. The time resolution is probe-wavelength dependent; in these experiments, the fwhm of the instrument response function (IRF) varied between 140 and 200 fs (e.g., at 680 nm, the IRF was 150 ± 6 fs).

Nanosecond Transient Absorption Experiments. The transient absorption setup for accessing microsecond delay times, housed at the Regional Laser and Biotechnology Laboratory at the University of Pennsylvania (RLBL), has been described previously.[89] The excitation wavelength for all samples was 532 nm. Samples were prepared in 1 cm quartz cells using distilled, dry acetonitrile, which was degassed by five

Scheme 1. General Synthetic Scheme for RuPZn-Based Chromophores

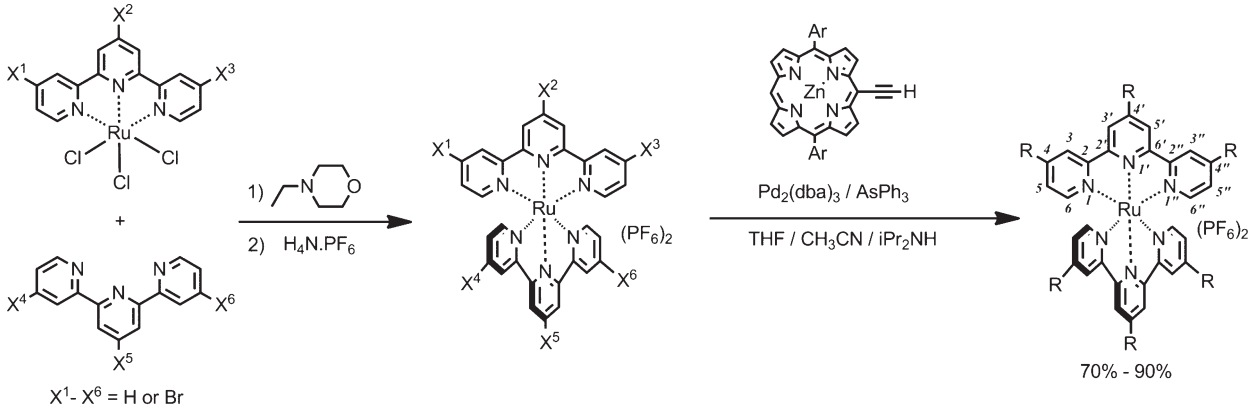

Precursor **10**: X^1 = Br, $X^2 = X^3 = X^4 = X^5 = X^6$ = H, **11**: $X^2 = X^5$ = Br, $X^1 = X^3 = X^4 = X^6$ = H,
12: $X^2 = X^4$ = Br, $X^1 = X^3 = X^5 = X^6$ = H, **13**: $X^1 = X^4$ = Br, $X^2 = X^3 = X^5 = X^6$ = H
14: $X^1 = X^3$ = Br, $X^2 = X^4 = X^5 = X^6$ = H, **15**: $X^2 = X^4 = X^6$ = Br, $X^1 = X^3 = X^5$ = H
16: $X^1 = X^4 = X^6$ = Br, $X^2 = X^3 = X^5$ = H, **17**: $X^1 = X^3 = X^4 = X^6$ = Br, $X^2 = X^5$ = H

successive freeze−pump−thaw cycles. Excited-state lifetimes were calculated by performing an exponential fit to the decay or the ground-state bleach rise of each respective compound. Each sample was run multiple times at various concentrations to ensure that other deactivation pathways were not present.

Hyper Rayleigh Light Scattering (HRS) Measurements. Femtosecond HRS experiments were performed at 1300 nm.[90,91] The chromophores were dissolved in acetonitrile and passed through 0.2 μm filters. Disperse red 1 (DR1, $\beta_{800} = 54 \times 10^{-30}$ esu in $CHCl_3$)[91] was utilized as a reference chromophore. For these external references in different solvents, standard local field correction factors were applied $[((n_D^2 + 2)/3)^3]$, where n is the refractive index of the solvent at the sodium D line]. Note that these experiments were performed at low chromophore concentrations where the linearity of the HRS signal as a function of chromophore concentration confirmed that no significant self-absorption of the SHG signal occurred in these experiments. Depolarization ratios have also been obtained, to probe the symmetry of the nonlinear scatterer.[92,93]

The depolarization ratio ρ is determined as the intensity ratio $\rho = I_{\parallel}/I_{\perp} = \langle\beta_{ZZZ}{}^2\rangle/\langle\beta_{YZZ}{}^2\rangle$ between the HRS signal intensity (I) for parallel ($I_{\parallel}$) and perpendicular ($I_{\perp}$) polarization between incoming fundamental (vertically polarized along the macroscopic laboratory Z axis) and detected harmonic signal (polarized either along the same Z axis for parallel and along the Y axis for perpendicular polarization). In order to determine accurately this ratio, the analyzing polarizer in front of the detector is rotated and the total HRS signal intensity is recorded as a function of angle between the two polarization states. From a fitting to this periodic pattern, an accurate depolarization ratio can be determined.

Ru(tpy)[4-(Zn-porphyrin)ethynyl-tpy](PF$_6$)$_2$ (2). Zinc(II) 5-ethynyl-10,20-bis[2′,6′-bis(3,3-dimethyl-1-butyloxy)phenyl]porphyrinate (19.4 mg, 0.0204 mmol) and **10** (Scheme 1, 20.2 mg, 0.0216 mmol) were placed into a 25 mL Schlenk tube with a stir bar. Trisdibenzylideneacetone dipalladium(0) (2.9 mg, 3.2 μmol) and triphenylarsine (3.6 mg, 0.012 mmol) were added, followed by dry THF (2.5 mL), CH_3CN (5.0 mL) and iPr_2NH (0.8 mL); this mixture was completely degassed by repeated freeze−pump−thaw cycles. The Schlenk tube was refilled with Ar gas, and the reaction mixture was stirred at 70 °C for 24 h. The reaction mixture was cooled to rt and the solvent evaporated. The residue was purified by column chromatography on silica gel eluted with a mixed solvent system [CH_3CN:H_2O:KNO_3 (aq) = 90:9:1]. The second green-brown fraction was collected and evaporated. The residual dark brown solid was dissolved in CH_3CN, and excess ammonium hexafluorophosphate and H_2O were added. Dark brown crystals of **2** (25.8 mg, 14.3 μmol, 70% yield) were collected by filtration. ^{1}H NMR (CD_3CN): δ 10.09 (s, 1H, *meso*-H), 9.64 (m, 2H, β-H), 9.23 (m, 2H, β-H), 9.03 (d, J = 8.0 Hz, 2H, 6-py), 8.87 (d, J = 4.5 Hz, 2H, β-H), 8.81 (m, 3H), 8.77 (d, J = 4.5 Hz, 2H, β-H), 8.54 (m, 4H), 8.47 (t, J = 8.0 Hz, 1H, 4-py), 7.96 (m, 3H), 7.79 (t, J = 8.5 Hz, 2H, *-p*-Ph), 7.45 (d, J = 7.5 Hz, 2H, 3 and 3′′-Py*H* for tpy), 7.44 (d, J = 8.0 Hz, 1H, 3′′-Py*H* for 4-PZn-tpy), 7.22 (m, 5H), 7.14 (d, J = 8.5 Hz, 4H, *-m*-Ph), 3.94 (t, J = 7.0 Hz, 8H, $-OCH_2-$), 0.74 (t, J = 7.0 Hz, 8H, $-CH_2CH_2-$), 0.13 (s, 36H, $-CH_3$). ^{19}F NMR (CD3CN): δ −71.67 (d, J = 752 Hz). UV−vis (CH_3CN): λ_{max} [nm] (ε [x 10^{-5} $M^{-1}cm^{-1}$]) 311 (0.58), 445 (1.18), 565 (0.14), 636 (0.35). MS (MALDI-TOF) m/z: 1513 (calcd for $C_{88}H_{88}N_{10}O_4RuZn$ $(M - 2PF_6)^+$ 1514) and 1659 (calcd for $C_{88}H_{88}N_{10}O_4F_6PRuZn$ $(M - PF_6)^+$ 1659).

Ru[4′-(Zn-porphyrin)ethynyl-tpy]$_2$(PF$_6$)$_2$ (3), Ru[4-(Zn-porphyrin)ethynyl-tpy][4′-(Zn-porphyrin)ethynyl-tpy](PF$_6$)$_2$ (4), Ru[4-(Zn-porphyrin)ethynyl-tpy]$_2$(PF$_6$)$_2$ (5), Ru(tpy)[4,4′′-bis(Zn-porphyrin)ethynyl-tpy](PF$_6$)$_2$ (6), Ru[4′-(Zn-porphyrin)ethynyl-tpy][4,4′′-bis(Zn-porphyrin)ethynyl-tpy](PF$_6$)$_2$ (7), Ru[4-(Zn-porphyrin)ethynyl-tpy][4,4′′-bis(Zn-porphyrin)ethynyl-tpy](PF$_6$)$_2$ (8), and Ru[4,4′′-bis(Zn-porphyrin)ethynyl-tpy]$_2$(PF$_6$)$_2$ (9). These compounds were synthesized using synthetic methods similar to that described for compound **2**. Detailed synthetic procedures and corresponding characterization data for chromophores **3**−**9** can be found in the Supporting Information.

RESULTS AND DISCUSSION

Synthesis and Design. Figure 1 highlights a series of mono-, bis-, tris-, and tetrakis(porphinato)zinc(II) (PZn)-elaborated ruthenium(II) bis(terpyridine) (Ru) complexes in which an ethyne unit connects the macrocycle *meso* carbon atom to terpyridyl (tpy) 4-, 4′- and 4′′-positions. These species were synthesized in high yield from appropriately ethynylated porphyrinic and halogenated ruthenium bis(tpy) precursor molecules via metal-catalyzed cross-coupling reactions (Schemes 1 and 2).[25,34,94−100] All compounds were isolated via column chromatography on silica gel; following counterion metathesis with ammonium hexafluorophosphate, the corresponding bis(hexafluorophosphate) salts were isolated, which were used for all spectroscopic experiments. The Figure 1 compounds show structures that range in complexity from the dipolar D−Br−A chromophore [PZn-(4′Ru)] (**1**) to the highly substituted symmetrical, yet non-centrosymmetric,

Scheme 2. Reaction Scheme Outlining the Evolution of NLO Octopoles from Dipolar Chromophoric Building Blocks

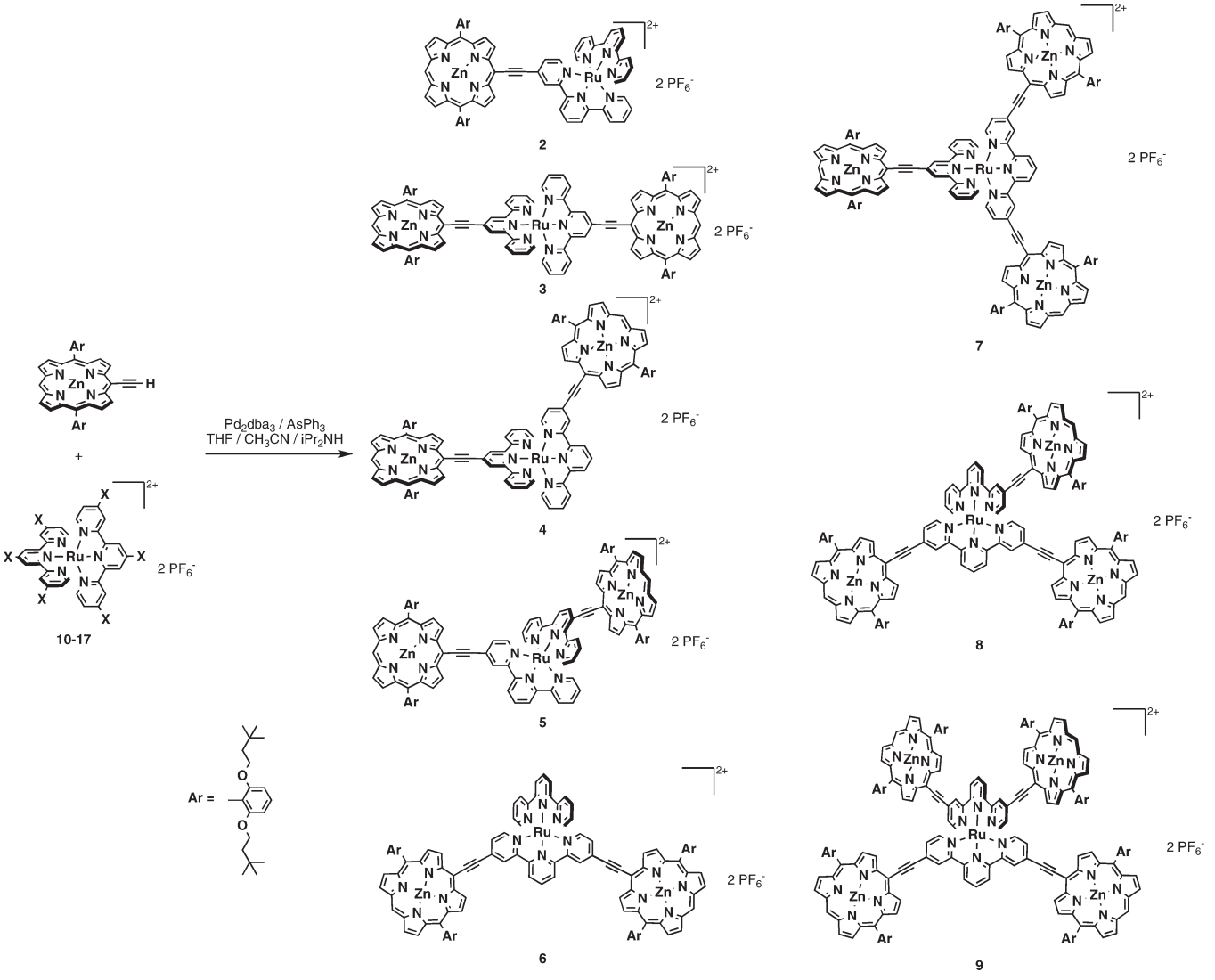

$(PZn)_2$-(4,4″Ru4,4″)-$(PZn)_2$ (**9**), which possesses four 5-ethynyl-(porphinato)zinc(II) substituents arranged about a $Ru(tpy)_2$ core.

Electronic Absorption Spectroscopy. The electronic absorption spectra (EAS) of these species (Figure 2, Table 1) evince strong mixing of the PZn-based oscillator strength with ruthenium terpyridyl charge resonance bands. Note that the EAS of supermolecular chromophores **1**−**9** differ markedly from those of the monomeric 5-ethynyl-PZn and $[Ru(tpy)_2]^{2+}$ building blocks.[25,45] It is important to highlight, however, that supermolecular chromophores **1**−**9** retain spectral qualities that trace their genesis to those of classical PZn and $[Ru(tpy)_2]^{2+}$ oscillators. For instance, **1**−**9** evince (i) a strong (ε > 100,000 M^{-1} cm^{-1}) absorption near ∼450 nm which features significant porphyrin-derived $^1\pi-\pi^*$ Soret (B) band character; (ii) a visible band centered at ∼510 nm which exhibits significant $[Ru(tpy)_2]^{2+}$-derived singlet metal-to-ligand charge transfer (^{1}MLCT) character and marked contributions from porphyrin ligand oscillator strength; and (iii) bands localized at ∼567 and ∼650 nm which exhibit porphyrinic $^1\pi-\pi^*$ Q-state character, with the lower energy, *x*-polarized transition manifesting features due to symmetry breaking and oscillator strength redistributions that derive from conjugation expansion[21,22,101] and charge resonance character that originates from the ethyne-bridged porphyrin *meso*-carbon-to-terpyridyl-carbon linkage.[25,45] Note that, in order to facilitate comparison of the spectral properties of these conjugated supermolecules with those of traditional (porphinato)zinc(II) and (polypyridyl)metal(II) benchmarks, MLCT (d−π^*), Soret (B)- and Q-band ($\pi-\pi^*$) state and transition labels are preserved throughout this report. When these terms are used in reference to the absorption bands of these RuPZn-based chromophores, they denote only the dominant contributor to the oscillator strength of the transition in question; it is recognized that MLCT, ligand, Soret, and Q electronic states mix extensively in these supermolecules.[102]

Examination of the Figure 2 spectra reveals that 4′-tpy attachment facilitates the strongest mixing of the PZn B_x (i.e., polarized along the long molecular axis defined by the ethynyl moiety) and metal polypyridyl charge-resonance states, giving rise to an enhanced singlet metal-to-ligand (^{1}MLCT) transition evident at ∼510 nm in the spectra of compounds **1**, **3**, **4**, and **7**, relative to analogous chromophores (**2**, **5**, **6**, **8**, and **9**) that feature 4 and 4″ PZn-to-tpy linkage topologies. It is important to stress, however, that these ^{1}MLCT transitions centered near 510 nm for

dx.doi.org/10.1021/ja105004k |*J. Am. Chem. Soc.* 2011, 133, 2884–2896

chromophores **1**−**9** all feature significant PZn-based oscillator strength contributions (Figure 2). Other than these modest spectral differences in the ^{1}MLCT band, remarkable spectral similarity is evident in the B- and Q-derived manifolds for **1**−**9**.

The Figure 2 spectra likewise indicate that multiple PZn moieties linked via ethynes to a $[Ru(tpy)_2]^{2+}$ core do not give rise to appreciable electronic coupling between PZn units, regardless of whether they are located on the same or opposite terpyridine ligand (compounds **3**−**9**). The absorption oscillator strengths of the porphyrin-dominated bands scale roughly with the number of macrocycles (Table 1), though the strong mixing of MLCT, tpy ligand, Soret, and Q electronic states makes rigorous quantification difficult. Note that as none of the hallmarks of strongly coupled multiporphyrin systems (e.g., dramatic transfer of oscillator strength from the B- band to the Q-band, and strong Q-band red-shifting),[34,35,37−39,41,42,44,46,48,50,52,103−107] are evident in the EAS of compounds **3**−**9**, it is reasonable to view the observed spectral properties of these supermolecules as deriving from a simple composite of multiple RuPZn oscillators. Congruent with this, note that the oxidative and reductive electrochemical data (Table 2) indicate that the potentiometric responses observed for **1**−**9** trace their origin largely to established $[Ru(tpy)_2]^{2+}$- and PZn-localized redox processes. These key ground-state absorptive spectroscopic features and potentiometric characteristics make possible the evolution of NLO octopoles from the dipolar RuPZn chromophoric archetype (*vide infra*).

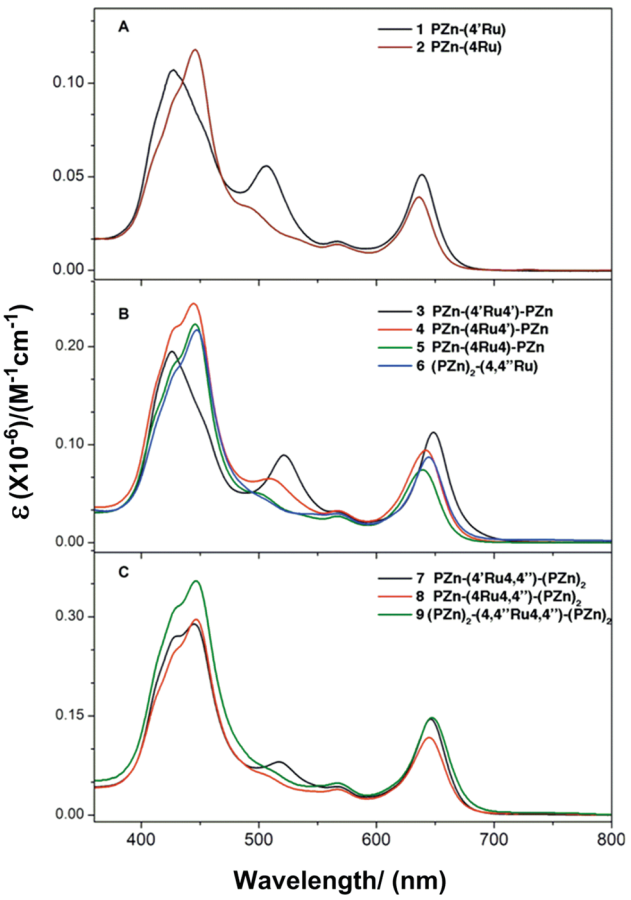

Figure 2. Comparative electronic absorption spectra of: (A) PZn-(4′Ru) (**1**) and PZn-(4Ru) (**2**); (B) PZn-(4′Ru4′)-PZn (**3**), PZn-(4Ru4′)-PZn (**4**), PZn-(4Ru4)-PZn (**5**), and $(PZn)_2$-(4,4″Ru) (**6**); (C) PZn-(4′Ru4,4″)-$(PZn)_2$ (**7**), PZn-(4Ru4,4″)-$(PZn)_2$ (**8**), and $(PZn)_2$-(4,4″Ru4,4″)-$(PZn)_2$ (**9**) in CH_3CN solvent.

Excited State Dynamics. Pump−probe transient absorption spectroscopic studies of this entire class of compounds (chromophores **1**−**9**) demonstrate that all of these species exhibit excited-state dynamical characteristics and transient spectral features similar to those reported for PZn-(4′Ru) (**1**, Figure 1).[45,48] In this regard, it is important to note that the excited-state relaxation dynamics of PZn-(4′Ru), and those established for closely related structures,[45,48] exhibit marked differences from those delineated for their component chromophoric building blocks (PZn and $[Ru(tpy)_2]^{2+}$). Monomeric (porphinato)zinc(II) compounds generally relax through both the singlet and triplet manifolds, leading to deactivation on both the nanosecond (singlet) and millisecond (triplet) time scales;[42] at room temperature, the initially prepared $[Ru(tpy)]^{2+}$ electronically excited state rapidly crosses to the low-lying metal-to-ligand charge transfer (triplet) surface,[108−110] where fast quenching dynamics driven by thermal population of a low-lying ^{3}MC state results in a ^{3}MLCT lifetime of only ∼250 ps at 298 K.[111] In PZn-(4′Ru),[45,48] transient absorption spectra obtained at early time delays (t_{delay} < 400 fs) demonstrate fast excited state relaxation, and manifest the characteristics of a highly polarized T_1 excited state; the combined effects of rapid intersystem crossing and strong coupling to

Table 1. Electronic Spectral Data for Ru-PZn Derivatives

	abs band maxima [nm] ($\varepsilon \times 10^{-5}$ [M^{-1} cm^{-1}])				oscillator strength		
	B-band[a]	^{1}MLCT[a]	Q-bands[a]		B-band region[a,b]	Q-band region[a,c]	total[d]
PZn-(4′Ru) (**1**)	428 (1.07)	506 (0.56)	567 (0.15)	639 (0.51)	2.10	0.27	2.37
PZn-(4Ru) (**2**)	445 (1.18)		565 (0.14)	636 (0.35)	1.90	0.25	2.15
PZn-(4′Ru4′)-PZn (**3**)	426 (1.95))	521 (0.89)	565 (0.32)	648 (1.13)	3.55	0.67	4.22
PZn-(4Ru4′)-PZn (**4**)	445 (2.44)	509 (0.65)	567 (0.32)	642 (0.95)	4.28	0.60	4.88
PZn-(4Ru4)-PZn (**5**)	446 (2.23)		566 (0.27)	639 (0.75)	3.62	0.46	4.08
(PZn)2-(4,4″Ru) (**6**)	447 (2.17)		564 (0.30)	644 (0.87)	3.55	0.57	4.12
PZn-(4′Ru4,4″)-(PZn)2 (**7**)	445 (2.89)	517 (0.80)	565 (0.42)	646 (1.43)	5.23	0.81	6.07
PZn-(4Ru4,4″)-(PZn)2 (**8**)	446 (2.96)		565 (0.39)	644 (1.16)	4.96	0.72	5.68
(PZn)2-(4,4″Ru4,4″)-(PZn)2 (**9**)	446 (3.54)		566 (0.49)	647 (1.48)	6.12	0.96	7.09

[a] Transition labels denote the dominant contributor to the absorption manifold. [b] Oscillator strengths calculated over the 360 → 555 nm wavelength domain. [c] Oscillator strengths calculated over the 555 → 850 nm wavelength domain. [d] Oscillator strengths calculated over the 360 → 850 nm wavelength domain.

dx.doi.org/10.1021/ja105004k |*J. Am. Chem. Soc.* 2011, 133, 2884–2896

Table 2. Oxidative and Reductive Cyclic Voltammetric Data for Ru-PZn Derivatives[a]

	$E_{1/2}$ values (V)[d,e,f]						
		$Ru^{2+/3+}$	$PZn^{+/2+}$	$PZn^{0/+}$	$(tpy)^{-/0}$	$PZn^{-/0}$	$(tpy)^{-/2-}$
PZn-(4′Ru) (**1**)[b]		1.47	1.13	0.87	−1.07	−1.37	−1.58
PZn-(4Ru) (**2**)[c]		1.32	1.05	0.77	−1.03	−1.22	−1.40
PZn-(4′Ru4′)-PZn (**3**)[c]		1.42	1.10	0.75	−1.07	−1.39	
PZn-(4Ru4′)-PZn (**4**)[c]		1.41	1.24	0.78	−1.09	−1.39	−1.55
PZn-(4Ru4)-PZn (**5**)[c]		1.38	1.23	0.76	−1.08	−1.26	−1.51
$(PZn)_2$-(4,4′′Ru) (**6**)[c]		1.40	1.21	0.77		−1.37	−1.57
PZn-(4′Ru4,4′′)-$(PZn)_2$ (**7**)[c]		1.43	1.23	0.82		−1.30	−1.53
PZn-(4Ru4,4′′)-$(PZn)_2$ (**8**)[c]	1.74	1.44	1.24	0.82		−1.28	−1.40
$(PZn)_2$-(4,4′′Ru4,4′′)-$(PZn)_2$ (**9**)[c]		1.49	1.21/1.05	0.87/0.78		−1.19	

[a] Experimental conditions: [complex] = 1 mM; electrolyte = 0.1 M $TBAPF_6$; scan rate = 100 mV/s; working electrode = Pt disk. [b] Solvent = CH_2Cl_2. [c] Solvent = CH_3CN. [d] $E_{1/2}$ values are relative to SCE. [e] ΔE_p values: $\Delta E_p(Ru^{2+/3+}) \sim 100$ mV; $\Delta E_p(PZn^{+/2+}) \sim 125$ mV; $\Delta E_p(PZn^{0/+}) \sim 100$ mV; under these experimental conditions, ΔE_p(ferrocene/ferrocenium = 100 mV). [f] Potentiometric data reported for $(tpy)^{-/0}$, $PZn^{-/0}$, and $(tpy)^{-/2-}$ redox processes correspond to E_{pc} values as these electrode-coupled reactions evince varying degrees of chemically irreversible character.

low-lying MLCT states gives rise to excited-state lifetimes on the order of tens of microseconds. Interrogation of the electronically excited states of PZn-(4′Ru) and related chromophores via pump−probe transient optical methods reveals a number of conspicuous spectral characteristics that include (i) prominent visible region bleaching due to ground-state depletion, (ii) a broad, weak transient absorption in the spectral region between the high oscillator ground-state bleaches, and (iii) an expansive, intense $T_1 \rightarrow T_n$ absorption manifold that dominates the 800−1200 nm region of the NIR.[45,48]

Figure 3 highlights exemplary transient absorption spectral data for chromophores **2** and **7** obtained over a 200 fs (fs) to 3 ns (ns) time domain. These data typify many of the time-dependent transient absorption spectral signatures characteristic for chromophores **1**−**9** and highlight the multiexponential nature of their relaxation dynamics. Supermolecules **1**−**9** manifest an ∼10−20 ps time constant component that leads to an increase in the intensity of the $T_1 \rightarrow T_n$ NIR transient absorption band; these dynamics are associated with torsional motion about the ethynyl bridge.[40,45,48,112] The relaxed ^{3}MLCT states of these species feature conformeric distributions having a reduced mean torsional angle between the porphyrin and terpyridine least-squares planes; moreover, the distribution of these torsional angles in the relaxed excited states of **1**−**9** is more homogeneous than that for their respective initially prepared excited states. Note that these relaxed excited triplet states thus display augmented $T_1 \rightarrow T_n$ manifold transition oscillator strengths with respect to that evident in the respective initially prepared ^{3}MLCT states of these structures.[45,48]

The excited-state dynamics elucidated for PZn-(4Ru), however, show a number of differences relative to those determined for chromophores **1** and **3**−**9**; some of these dissimilarities can be recognized in the Figure 3 data. While the excited state dynamical data acquired for PZn-(4Ru) (**2**, Figure 3A) bear some resemblance with those reported for PZn-(4′Ru),[45,48] note that PZn-(4Ru) does not manifest a prominent ^{1}MLCT band in its ground-state absorption spectrum (Figure 2). As a result, more complex features are evident throughout the 700−800 nm spectral domain over the initial few picoseconds following excitation of this complex (Figure 3A), contrasting that reported earlier for related chromophores,[45,48] and that observed in the analogous dynamical data acquired for supermolecules **3**−**9** (see for example the chromophore **7** transient spectra of Figure 3B). A global exponential fit to the PZn-(4Ru) transient absorption data acquired at multiple wavelengths produces time constants of 1.7 and 18.9 ps; while the latter component corresponds to the torsional dynamics described above, the 1.7 ps component is associated with the simultaneous decay of the absorption feature observed over 700−800 nm spectral window characteristic of the initially prepared excited state, and the growth of the NIR absorption manifold (900−1200 nm).

The transient absorption signal observed over the 700−800 nm spectral region suggests an initially prepared excited state for **2** that possesses significantly less electronic delocalization than its corresponding relaxed state. As evinced in the steady state absorption spectra (Figure 2), the 4′-tpy-to-5-ethynyl(porphinato) zinc linkage topology facilitates stronger mixing of PZn B_x and metal polypyridyl charge-resonance states relative to those that utilize corresponding 4- and 4′′-connectivities. Congruent with the suggestion that linkage-topology-dependent differences in electronic coupling may play a role in determining excited-state dynamics, electronic structure calculations indicate that the tpy 4- and 4′′-positions manifest diminished electron density relative to the 4-carbon atom in the $Ru(tpy)_2$ LUMO.[113] A qualitative analysis based on the Table 2 potentiometric data and the Gibbs free energy relation suggests that reaction thermodynamics may play a role as well in limiting the extent of electronic delocalization evidenced in the PZn-(4Ru) excited state probed at t_{delay} = 200 fs, relative to that manifest for chromophores **1** and **3**−**9** at an identical time delay.[114] Whatever the origin of these apparent differences in **2**'s initially prepared excited state, picosecond time scale spectral evolution gives rise to a high oscillator strength $T_1 \rightarrow T_n$ NIR transient absorption manifold qualitatively indistinguishable from that observed for the initially prepared electronically excited states of related supermolecules **1** and **3**−**9**. Note that, in this family of chromophores, the lifetimes of the relaxed ^{3}MLCT states are on the order tens of microseconds.

Table 3 tabulates excited-state lifetimes and the $T_1 \rightarrow T_n$ absorption extinction coefficients for **1**−**9**; note that these estimated $T_1 \rightarrow T_n$ extinction coefficients are calculated from spectra acquired at 1.5 ns following excitation, and were determined by comparing the excited state absorption to the Q_x-band-derived ground state bleach (having a known extinction coefficient), following a method detailed previously.[45] As the

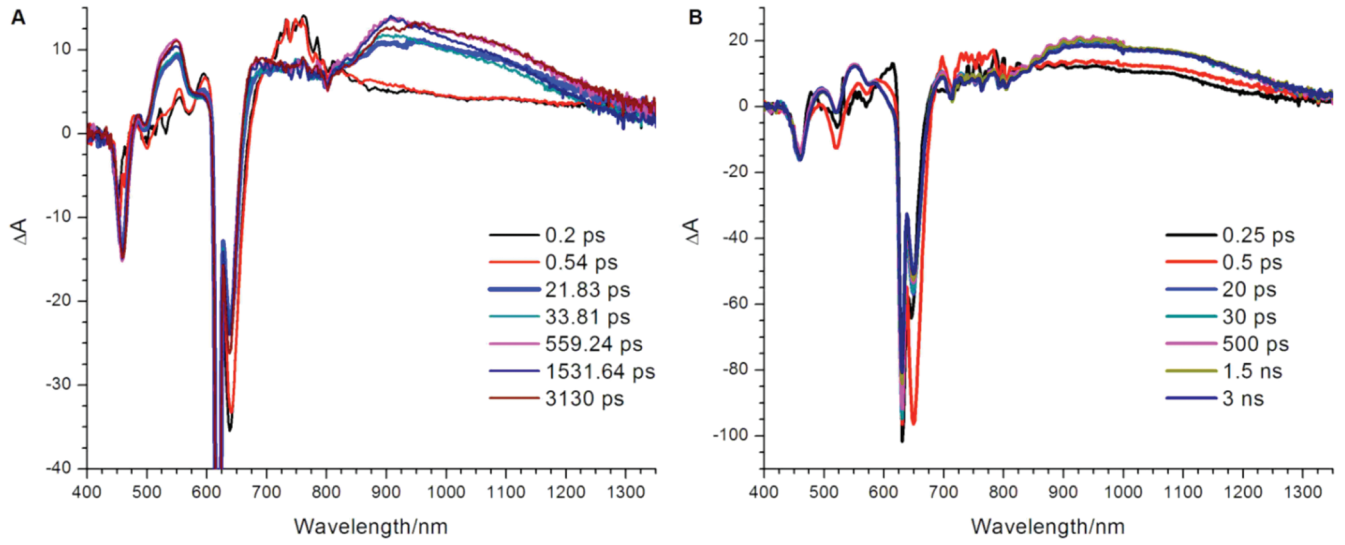

Figure 3. Magic angle pump−probe transient absorption spectra of compounds **2** (A) and **7** (B), recorded at several time delays illustrating the general transient features of chromophores **1**−**9**. Note that the NIR absorption manifold is strongly established at a time delay of 250 fs in compound **7** (as well as in chromophores **1**, **3**−**6**, and **8** and **9**), but not in compound **2**. The laser line from the pump pulse at 605 nm is observed in both spectra. Experimental conditions: solvent = acetonitrile, ambient temperature, λ_{exc} = 605 nm.

Table 3. Excited-Triplet State Data for 1−9[a]

	λ_{max} $(T_1 \rightarrow T_n)$[b] (nm)	extinction coeff, $\lambda_{max}(T_1 \rightarrow T_n)$ $[M^{-1}\ cm^{-1}]$[b,c]	triplet lifetimes (μs)
PZn-(4′Ru) (**1**)	884	29900	44[d]
PZn-(4Ru) (**2**)	908	18200	73
PZn-(4′Ru4′)-PZn (**3**)	900	44400	33
PZn-(4Ru4′)-PZn (**4**)	909	48200	44
PZn-(4Ru4)-PZn (**5**)	926	38600	26
$(PZn)_2$-(4,4′′Ru) (**6**)	917	26200	82
PZn-(4′Ru4,4′′)-$(PZn)_2$ (**7**)	938	54000	33
PZn-(4Ru4,4′′)-$(PZn)_2$ (**8**)	930	48200	61
$(PZn)_2$-(4,4′′Ru4,4′′)-$(PZn)_2$ (**9**)	957	67100	14

[a] All spectral data were acquired in acetonitrile solvent. [b] $\lambda_{max}(T_1 \rightarrow T_n)$ corresponds to the $T_1 \rightarrow T_n$ manifold absorption having the largest extinction coefficient at t_{delay} = 1.5 ns. [c] Excited state extinction coefficients were estimated using a method described previously.[45] [d] Electronically excited triplet data for **1** reported previously.[45]

NIR absorption manifold clearly consists of many transitions, the λ_{max} value reported corresponds to the extinction coefficient of the absorption maximum located in the higher-energy portion of the $T_1 \rightarrow T_n$ manifold. Note that $\lambda_{max}(T_1 \rightarrow T_n)$ increases with increasing numbers of 5-ethynyl-(porphinato)zinc(II) substituents connected to the $Ru(tpy)_2$ core (e.g., **1**, $\lambda_{max}(T_1 \rightarrow T_n)$ = 884 nm; **4**, $\lambda_{max}(T_1 \rightarrow T_n)$ = 909 nm; **7**, $\lambda_{max}(T_1 \rightarrow T_n)$ = 930 nm; **9**, $\lambda_{max}(T_1 \rightarrow T_n)$ = 957 nm). While this may signal a modest degree of excited-state electronic delocalization involving multiple RuPZn units, it is important to underscore that the overall $T_1 \rightarrow T_n$ absorption bandwidth and normalized intensity are virtually identical for chromophores **1**−**9**; along this line, note that the extinction coefficient of $\lambda_{max}(T_1 \rightarrow T_n)$ normalized by the number of (porphinato)zinc(II) units is roughly constant (~20,000 $M^{-1}\ cm^{-1}$) throughout these supermolecules.

Congruent with insights derived from electronic spectral and potentiometric data, these transient absorption spectral studies further support the notion that the individual RuPZn fragments of chromophores **3**−**9** exhibit, at best, only modest excited-state electronic interactions that derive from factors other than the dipolar interactions of the component RuPZn oscillators. Because the nature of the chromophore electronically excited states present at early and long delay times are reminiscent of that previously established for PZn-(4′Ru) (**1**),[45,48] the electronically excited states of supermolecules **3**−**9** can thus be approximated as a collection of interacting RuPZn transition dipoles that to first order behave as independent oscillators. While a detailed description would certainly need to consider excitation delocalization via energy transfer and the impact of conformational dynamics upon these excited states, the electronic structural data for **1**−**9** that emerge from these pump−probe transient absorption experiments indicate fundamentally sound design principles underpinning these structures: because the nature of the instantaneously prepared excited states determine the virtual states that govern the NLO response, the approximate independent character of the component RuPZn oscillators for **3**−**9** suggest nonlinear optical responses for these supermolecules consistent with those defined for multipolar chromophores (*vide infra*).

Nonlinear Optical Properties. Chromophores **1**−**9** possess large CT transition oscillator strengths (P_{ge}s) and substantial dipole moment differences between their respective ground and excited electronic states ($\Delta\mu_{ge}$s). How these parameters *qualitatively* impact the magnitude or the dynamic hyperpolarizability can be seen in classic two-level formulation of β (eq 1), where β'_n refers to an electronic-state specific two-level contribution to the sum-over-states expression for β, E_{op} refers to a specific electronic transition energy and E_{inc} is the incident irradiation energy.[11,12]

$$\beta'_n = \frac{6(P_{ge})_n^2(\Delta\mu_{ge})_n(E_{op})_n^2}{[(E_{op})_n^2 - (2E_{inc})^2][(E_{op})_n^2 - E_{inc}^2]} \qquad (1)$$

These Ru-PZn-based species manifest complex nonlinear responses because of the coupling among the electronic transitions of the chromophoric building blocks (i.e., three-level

dx.doi.org/10.1021/ja105004k |*J. Am. Chem. Soc.* 2011, 133, 2884–2896

Table 4. Dynamic Hyperpolarizabilities [β_{1300}, ($\times 10^{-30}$ esu)] and Depolarization Ratios (ρ) Determined by Hyper-Rayleigh Experiments[a]

	β_{ijk}[b]	β_{HRS}	ρ[c]
PZn-(4′Ru) (**1**)	5100[d]	2100	3.8 ± 0.1
PZn-(4Ru) (**2**)	3100 ± 50	1280 ± 20	3.8 ± 0.1
PZn-(4′Ru4′)-PZn (**3**)	1920 ± 70	800 ± 30	3.9 ± 0.1
PZn-(4Ru4′)-PZn (**4**)		880 ± 30	2.2 ± 0.1
PZn-(4Ru4)-PZn (**5**)		960 ± 30	2.1 ± 0.1
$(PZn)_2$-(4,4′′Ru) (**6**)		1080 ± 40	3.4 ± 0.1
PZn-(4′Ru4,4′′)-$(PZn)_2$ (**7**)		750	2.1 ± 0.2
PZn-(4Ru4,4′′)-$(PZn)_2$ (**8**)		894	2.1 ± 0.2
$(PZn)_2$-(4,4′′Ru4,4′′)-$(PZn)_2$ (**9**)	1380 ± 260[118]	1040 ± 200	1.5 ± 0.1

[a] λ_{inc} = 1300 nm. [b] $\beta_{ijk} = \beta_{zzz}$ for upper 3 entries with dipolar molecular symmetry ($\rho \sim 4$) and $\beta_{ijk} = \beta_{xyz}$ for last entry (**9**) having effective octopolar symmetry ($\rho = 1.5$); $\beta_{HRS}^2 = [\langle\beta_{ZZZ}^2\rangle + \langle\beta_{YZZ}^2\rangle] = 6/35\ \beta_{zzz}^2$ for dipolar compounds, and $\beta_{HRS}^2 = [\langle\beta_{ZZZ}^2\rangle + \langle\beta_{YZZ}^2\rangle] = 20/35\ \beta_{xyz}^2$ for octopolar (T_d, D_2, or D_{2d}) symmetries;[118] [c] $\rho = \langle\beta_{ZZZ}^2\rangle/\langle\beta_{YZZ}^2\rangle$; [d] Value taken from ref 25.

contributions arising from mixing of transitions that trace their genesis to (porphinato)zinc B- and Q-states and metal polypyridyl ligand-to-metal CT states).[18,25,48] Because multiple absorption manifolds contribute to the nonlinear response and the transitions that dominate these manifolds possess distinct transition dipole directions, chromophores **1**−**9** manifest complex frequency dispersions of the hyperpolarizability. As excited state-to-excited state transition dipoles play such a prominent role in determining the NLO responses of Ru-PZn-based chromophores, two-level analyses such as that described in eq 1 provide only a qualitative understanding of the frequency dispersion of β_λ. This issue has recently been discussed in detail, and the frequency dispersion of the hyperpolarizability for chromophores within this family has been analyzed using a sum-over-states expression with three-level contributions that employed measured spectroscopic parameters and generalized Thomas−Kuhn sum rules.[18]

Table 4 lists dynamic hyperpolarizability (β_λ) values and depolarization ratios (ρ) determined from hyper-Rayleigh light scattering (HRS) measurements carried out at an incident irradiation wavelength (λ_{inc}) of 1300 nm in CH_3CN solvent. Briefly, the depolarization ratio provides insight in to the nature of contributions to the NLO response.[31] For a purely octopolar compound, the depolarization ratio is predicted to be 1.5, while for a molecule with a single contributing major β_{zzz} hyperpolarizability tensor component, this value is 5.[115,116] This latter ρ value is attained only in the limit of an HRS experiment carried out using an infinitely small numerical aperture for a hypothetical chromophore that possesses no finite off-diagonal tensor contributions to β_λ for the experimental molecular symmetry. In practice, dipolar compounds exhibit a reduced depolarization value relative to this limiting theoretical value (e.g., for disperse red 1, a dipolar compound, ρ = 3.4); HRS depolarization ratios for classic octopolar chromophores such as 1,3,5-trihydroxy-2,4,6-trinitrobenzene and crystal violet have been determined to be 1.5.[63−77,117]

While it is well established that the depolarization ratio provides an experimental measure of chromophore optical symmetry, we note that this parameter provides an important experimental validation that appropriate coupling of multiple charge-transfer oscillators can be utilized to evolve the effective chromophore symmetry from purely dipolar to octopolar. Because excited-state dynamical, ground-state electronic absorption, and potentiometric data all point to the approximate independent character of the building block RuPZn oscillators of supermolecular chromophores **3**−**9**, for the purpose of analyzing the depolarization ratio data, it is useful to consider these species as assemblies of RuPZn dipoles. Insight into the nature of excited-state electron density distributions for **3**−**9** is thus gleaned through vector addition of these RuPZn dipoles. The geometric nature of the PZn substitution pattern about the $Ru(tpy)_2$ core of these chromophores determines the extent to which these dipoles add or cancel, which can be estimated by simple symmetry arguments. It is important to note that some of the supermolecular chromophore arrays do not, in fact, possess high molecular symmetry, due to the fact that the tpy 4- and 4′-(4′′-) positions are not electronically or chemically equivalent. In this electronic structural limit relevant to **3**−**9** where these strong RuPZn oscillators exhibit significant independent character, however, depolarization ratio measurements reveal the effective chromophore optical symmetry. This effective optical symmetry reflects the spatial arrangement of the RuPZn oscillators about the $Ru(tpy)_2$ core, that is, an approximate molecular symmetry that would exist if all points of connectivity to this unit were equivalent.

Depolarization ratio data compiled in Table 4 shows evolution of ρ values from dipolar ($\rho \sim 4$, chromophores **1**−**3**) to octopolar (ρ = 1.5, chromophore **9**). Given the lower approximate molecular symmetries of supermolecules **4**−**8**, intermediate values of ρ are manifest. Note that these ρ values correspond to depolarization ratios that are neither consistent with dipolar nor octopolar optical symmetry, but reflect the spatial arrangement of the component RuPZn oscillators of these species and the corresponding vector sums of these dipoles. Congruent with this, the small measured difference in the depolarization ratios for supermolecules **4** and **5**, which possess a similar relative spatial arrangement of their respective component RuPZn oscillators, yet different 5-ethynyl(porphinato)zinc-to-tpy linkage topologies, illustrates the utility of the notion of approximate molecular symmetry in rationalizing the relative magnitudes of ρ for compounds **4**−**9**. Given the electronic structural characteristics of **1**−**9** discussed above and the substantial RuPZn oscillator strength, the absolute nature of PZn-tpy connectivity (4, 4′, or 4′′) has little impact upon the determination of chromophore effective optical symmetry.

Consistent with the established NLO properties of RuPZn[25] and the dependence of chromophore effective optical symmetry upon structure, supermolecules **1**−**9** exhibit impressive second-order nonlinear optical responses at 1300 nm. In Table 4, note that $\beta_{HRS}^2 = [\langle\beta_{ZZZ}^2\rangle + \langle\beta_{YZZ}^2\rangle]$ reflects the total HRS intensity (i.e., the total magnitude of the HRS signal with polarization parallel and perpendicular to the Z-polarized fundamental laser beam), providing an average hyperpolarizability value that has not been analyzed toward specific hyperpolarizability tensor components for a specific molecular symmetry.[115,116] When considering these quantities, it is important to note the definitions of the *x*, *y*, and *z* axes, as the reference frame convention in the NLO community differs from that used to discuss the spectroscopic properties of these structures. β_{zzz} denotes a first hyperpolarizability tensor component along the dipolar molecular *z* axis for charge transfer; in contrast, β_{xxx}, for example, refers to one of the four nonzero hyperpolarizability tensor components for a D_{3h}-symmetric octopolar molecule in the *xy* plane, the

z axis again being the unique molecular axis perpendicular to this plane.

For the simple dipolar compounds, note that the β_{1300} value determined for PZn-(4′Ru) (**1**, $\beta_{HRS} = 2100 \times 10^{-30}$ esu) exceeds that of PZn-(4Ru) (**2**, $\beta_{HRS} = 1280 \times 10^{-30}$ esu); this result is consistent with the fact that 4′-tpy attachment facilitates the strongest mixing of the PZn B_x and metal polypyridyl charge-resonance states. In supermolecules **3**−**9**, which feature multiple RuPZn oscillators, the magnitude of β_{HRS} does not reflect such a dramatic difference between 4′ or 4 (4″) points of connectivity for the 5-ethynyl(porphinato)zinc units; this is likely due in part to symmetry dependent incomplete cancellation of dipolar contributions to the HRS response. In the more complex **3**−**9** superstructures, chromophore effective optical symmetry plays a critical role in determining the NLO response as underscored by the measured ρ values, and the relative impact of topological connectivity becomes less obvious.

With respect to the magnitude of the measured hyperpolarizability, note that the coupling of multiple RuPZn oscillators in the manner highlighted by the **3**−**9** structures not only evolves chromophore symmetry from dipolar to octopolar; Table 4 highlights that this mode of chromophore design gives rise to octopolar supermolecules that possess by far the largest off-diagonal octopolar first hyperpolarizability tensor components ever reported. $(PZn)_2$-(4,4″Ru4,4″)-$(PZn)_2$ (**9**), which features a 5-ethynyl(porphinato)zinc substitution pattern compatible with D_{2d} symmetry, shows complete cancellation of the vectorial dipolar contributions to the NLO response associated with its 4 component RuPZn oscillator fragments, and manifests a ρ value of 1.5, as expected for an ideal octopole. Note that chromophores **3**−**8**, which exhibit substantial variation in the magnitude of the measured depolarization ratio, display averaged hyperpolarizabilities (β_{HRS} values) that remain extremely large, independent of structure. These values range from 750 to 1080 $\times 10^{-30}$ esu, similar in magnitude to that determined for the octopolar supermolecule **9** ($\beta_{HRS} = 1040 \times 10^{-30}$ esu).

Because variations in molecular structure determine chromophore effective optical symmetry and lead to different nonzero hyperpolarizability tensor components contributing to the overall HRS response, the simplest comparative metric is the averaged hyperpolarizability, as discussed above. However, in order to contrast the HRS responses of these systems with key literature chromophoric benchmarks, the various tensor elements that contribute to the HRS response must be evaluated; such tensor-element-specific HRS responses for molecules of different symmetries can be compared directly. This approach is exemplified for $(PZn)_2$-(4,4″Ru4,4″)-$(PZn)_2$ (**9**), where $\beta_{HRS} = 1040 \times 10^{-30}$ esu and $\beta_{xyz} = 1380 \times 10^{-30}$ esu for the 6 contributing nonzero off-diagonal hyperpolarizability tensor components.[118] Supermolecule **9** exhibits the largest octopolar response reported, irrespective of symmetry or dispersion (frequency dependence of the response) considerations. Analyzing compound **9** NLO data within the context of effective D_{2d} symmetry, there are 6 nonzero tensor hyperpolarizability tensor elements β_{ijk}, $i \neq j \neq k$ that contribute to the total signal. With respect to comparisons of tensor-element-specific HRS responses, note that the relations between the observables are given by the following equations: $\beta_{HRS}^2 = [\langle\beta_{ZZZ}^2\rangle + \langle\beta_{YZZ}^2\rangle] = 6/35\ \beta_{zzz}^2$ for dipolar compounds, $\beta_{HRS}^2 = [\langle\beta_{ZZZ}^2\rangle + \langle\beta_{YZZ}^2\rangle] = 8/21\ \beta_{xxx}^2$ for octopolar D_{3h} symmetry, and $\beta_{HRS}^2 = [\langle\beta_{ZZZ}^2\rangle + \langle\beta_{YZZ}^2\rangle] = 20/35\ \beta_{xyz}^2$ for octopolar T_d, D_2, or D_{2d} symmetries.[118] This difference in prefactors for dipolar and octopolar symmetries (6/35 vs 8/21 or 20/35)[118] results in a seemingly small octopolar response (β_{HRS} value) for compound **9** compared to that determined for dipolar chromophores **1** and **2**. Calculating the tensor elements for an average $\beta_{HRS} = 1040 \times 10^{-30}$ esu for structures of different symmetries, it is easy to appreciate the extraordinary response of octopolar chromophore **9**. For a dipolar compound, a β_{zzz} value of 2500×10^{-30} esu would be needed to provide a corresponding $\beta_{HRS} = 1040 \times 10^{-30}$ esu; similarly, an octopolar, but D_{3h}, molecule would require $\beta_{xxx} = 1700 \times 10^{-30}$ esu to give rise to a β_{HRS} value exceeding 1000×10^{-30} esu.[115] This analysis provides a yardstick by which to compare molecules of different optical symmetries benchmarked to a specific second order response. Note that octopolar $(PZn)_2$-(4,4″Ru4,4″)-$(PZn)_2$ gives rise to a β_{HRS} value approximately equivalent to that for dipolar PZn-(4Ru) ($\beta_{zzz} = 3100 \times 10^{-30}$ esu), showing that it is possible to retain large NLO responses as the nature of the optical symmetry is modulated.

These considerations are important in the development of nonlinear optical materials based upon hyperpolarizable chromophores. The omnidirectional averaged response for molecules with high symmetry (yet non-centrosymmetry) results in a large nonlinear effect, as is observed for the 6 nonzero β_{ijk}, $i \neq j \neq k$ tensor components that contribute to the total average HRS signal observed for **9** ($\beta_{HRS} = 1040 \times 10^{-30}$ esu). A large off-diagonal β_{xyz} hyperpolarizability tensor component translates into an omnidirectional NLO response in a bulk materials and thin films, resulting in polarization insensitive devices that can be utilized as frequency-converters or electro-optic modulators.

It is important to underscore that the magnitude of the off-diagonal hyperpolarizability tensor component β_{xyz} for octopolar chromophore **9** (1380×10^{-30} esu)[118] was determined for a technologically important incident irradiation wavelength of 1300 nm. Pump−probe transient optical data evince that **1**−**9** are nonemissive; furthermore, the molecular hyperpolarizabilites determined for these species were acquired under experimental conditions that utilized classic fluorescence demodulation methods.[91,119] It is thus certain that the large β_{HRS} values reported herein are uncontaminated by multiphoton fluorescence contributions to the HRS signal. The largest octopolar β_{1300} value reported to date corresponds to structural analog of the $[Ru(bpy)_3]^{2+}$.[120,121] As HRS measurements for this chromophore at this irradiation wavelength are known to be heavily contaminated by multiphoton fluorescence, in order to provide a more accurate benchmark with which to compare to **9**, we note that β_{xxx} for this particular $[Ru(bpy)_3]^{2+}$ derivative determined at $\lambda_{inc} = 1900$ nm corresponds to 320×10^{-30} esu.[71] While multifluorescence contamination is always an issue when determining the hyperpolarizabilities of emissive chromophores, these concerns are somewhat mitigated at long irradiation wavelength. Projecting this β_{1900} value back to 1300 nm using the conventional dispersion relation gives $\beta_{xxx} = 500 \times 10^{-30}$ esu, and a corresponding averaged nonlinear response $\beta_{HRS} = 310 \times 10-30$ esu. The supermolecular chromophore $(PZn)_2$-(4,4″Ru4,4″)-$(PZn)_2$ thus possesses a β_{HRS} value at 1300 nm that is more than a factor of 3 larger than that determined for any chromophore having octopolar symmetry examined to date.

CONCLUSION

A new series of mono-, bis-, tris-, and tetrakis(porphinato)zinc-(II) (PZn)-elaborated ruthenium(II) bis(terpyridine) (Ru) complexes has been synthesized in which an ethyne unit connects

the macrocycle *meso* carbon atom to terpyridyl (tpy) 4-, 4′- and 4″-positions. These RuPZn-based species were synthesized in high yield from appropriately ethynylated porphyrinic and halogenated ruthenium bis(tpy) precursor molecules via metal-catalyzed cross-coupling reactions. While these supermolecular chromophores evince strong mixing of the PZn-based oscillator strength with ruthenium terpyridyl charge resonance bands, potentiometric and linear absorption spectroscopic data indicate that for structures in which multiple PZn moieties are linked via ethynes to a $[Ru(tpy)_2]^{2+}$ core, little electronic coupling is manifest between PZn units, regardless of whether they are located on the same or opposite tpy ligand. Congruent with these experiments, pump−probe transient absorption studies suggest that the individual RuPZn fragments of these structures exhibit, at best, only modest excited-state electronic interactions that derive from factors other than the dipole−dipole interactions of these strong oscillators. Because the nature of the instantaneously prepared excited states determines the virtual states that govern the nonlinear optical (NLO) response, the approximate independent character of the component RuPZn oscillators suggests that the design strategy described herein is ideal for designing NLO multipoles based on the potent dipolar hyperpolarizable RuPZn archetype.

Dynamic hyperpolarizability (β_λ) values and depolarization ratios (ρ) were determined from hyper-Rayleigh light scattering (HRS) measurements carried out at an incident irradiation wavelength (λ_{inc}) of 1300 nm. The depolarization ratio data provide an experimental measure of chromophore optical symmetry, and underscore that appropriate coupling of multiple charge-transfer oscillators evolves the effective chromophore symmetry from purely dipolar to octopolar. These effective chromophore optical symmetries were shown to depend solely upon the geometric nature of the PZn substitution pattern about the $Ru(tpy)_2$ core, highlighting that the NLO response derives from the collective properties of the component dipolar RuPZn supermolecular oscillators.[122] These chromophore design insights give rise to octopolar supermolecules that possess by far the largest off-diagonal octopolar first hyperpolarizability tensor components ever reported. The averaged hyperpolarizabilities (β_{HRS} values) for these species are extremely large, regardless of structure, ranging from 750 to 1080 $\times 10^{-30}$ esu. $(PZn)_2$-(4,4″Ru4,4″)-$(PZn)_2$, which possesses four 5-ethynyl-(porphinato)zinc(II) substituents arranged about a $Ru(tpy)_2$ core and rigorous octopolar symmetry, possesses the largest octopolar response ever reported, irrespective of symmetry or dispersion (frequency dependence of the response) considerations; importantly, its β_{HRS} value at 1300 nm (1040 $\times 10^{-30}$ esu) is more than a factor of 3 larger than that determined for any chromophore having octopolar symmetry examined to date. Because octopolar $(PZn)_2$-(4,4″Ru4,4″)-$(PZn)_2$ possesses six large off-diagonal β_{xyz} hyperpolarizability tensor components, large omnidirectional NLO responses can in principle be realized in both bulk materials and thin films, resulting in polarization insensitive devices that can be utilized as frequency-converters or electro-optic modulators.

This work demonstrates that ruthenium(II) [5-(4′-ethynyl-(2,2′;6′,2″-terpyridinyl))-10,20-bis(2′,6′-bis(3,3-dimethyl-1-butyloxy)phenyl)porphinato]zinc(II)-(2,2′;6′,2″-terpyridine)$^{2+}$ bis-hexafluorophosphate (RuPZn), a robust, benchmark dipolar chromophore that possesses an extraordinary β_{zzz} value at a telecommunication relevant wavelength (β_{1300} = 5100 $\times 10^{-30}$ esu), can not only serve as a template for the development of an octopolar NLO chromophore; appropriate coupling of multiple, related charge-transfer oscillators can be utilized to evolve the effective chromophore symmetry in RuPZn-based supermolecules from purely dipolar to octopolar, and generate octopolar NLO chromophores having impressive β_{HRS} values at 1300 nm (β_{HRS} > 1000 $\times 10^{-30}$ esu). Because NLO octopoles possess omnidirectional NLO responses while circumventing the electrostatic interactions that drive bulk-phase centrosymmetry for NLO dipoles at high chromophore concentrations, the advent of octopolar NLO chromophores having vastly superior β_{HRS} values at technologically important energies will motivate new experimental approaches to achieve acentric order in both bulk-phase and thin film structures.

■ ASSOCIATED CONTENT

Supporting Information. Syntheses and characterization data for precursor compounds, along with benchmark optical spectra for the ethyne-elaborated bis(terpyridyl)metal and (porphinato)zinc(II) building blocks. Complete author lists are provided for refs 58 and 59 This material is available free of charge via the Internet at http://pubs.acs.org.

■ AUTHOR INFORMATION

Corresponding Author

koen.clays@fys.kuleuven.be; michael.therien@duke.edu

Present Addresses

[‡]Department of Chemistry, Graduate School of Pure and Applied Sciences, University of Tsukuba, 1-1-1 Tennodai, Tsukuba 305-8571, Japan.

[§]Department of Biochemistry and Biophysics, University of Pennsylvania, School of Medicine, 316 Anatomy Chemistry Building, Philadelphia, PA 19104-6059.

■ ACKNOWLEDGMENT

This work was supported by a grant from the Department of Energy Biomolecular Materials program DE-FG02-04ER46156 (T.I., L.E.S, A.N., M.J.T.); K.S., S.-T.H., and K.C. are grateful to the Flemish Fund for Scientific Research (G.0312.08) and the University of Leuven (GOA/2006/03). The authors thank the MRSEC (DMR-00-79909) Program of the National Science Foundation, RLBL (NIH P41RR001348), and UNC EFRC - Solar Fuels and Next Generation Photovoltaics, an Energy Frontier Research Center funded by the U.S. Department of Energy, Office of Science, Office of Basic Energy Sciences, under Award Number DE-SC0001011, for infrastructural support. T.I. thanks the Japan Society for the Promotion of Science (JSPS) for a postdoctoral fellowship. M.J.T. is grateful to the Francqui Foundation (Belgium) and VLAC (Vlaams Academisch Centrum), Centre for Advanced Studies of the Royal Flemish Academy of Belgium for Science and the Arts, for research fellowships. The authors are indebted to Dr. Timothy V. Duncan for many helpful discussions.

■ REFERENCES

(1) Williams, D. J. *Angew. Chem., Int. Ed.* **1984**, *23*, 690–703.

(2) Beratan, D. N. In *New Materials for Nonlinear Optics*; Hann, R. A., Bloor, D., Eds.; ACS Symposium Series 455; American Chemical Society: Washington, DC, 1991; pp 89−102.

(3) Marder, S. R.; Beratan, D. N.; Cheng, L.-T. *Science* **1991**, *252*, 103–106.

(4) Prasad, P. N.; Williams, D. J. *Introduction to Nonlinear Optical Effects in Molecules and Polymers*; Wiley: New York, 1991.
(5) Ledoux, I.; Zyss, J.; Jutand, A.; Amatore, C. *Chem. Phys.* **1991**, *150*, 117–123.
(6) Chauchard, E.; Combellas, C.; Hendrickx, E.; Mathey, G.; Suba, C.; Persoons, A.; Thiebault, A. *Chem. Phys. Lett.* **1995**, *238*, 47–53.
(7) Verbiest, T.; Houbrechts, S.; Kauranen, M.; Clays, K.; Persoons, A. *J. Mater. Chem.* **1997**, *7*, 2175–2189.
(8) Marder, S. R.; Kippelen, B.; Jen, A. K.-Y.; Peyghambarian, N. *Nature* **1997**, *388*, 845–851.
(9) Dalton, L. R.; Steier, W. H.; Robinson, B. H.; Zhang, C.; Ren, A.; Garner, S.; Chen, A.; Londergan, T.; Irwin, L.; Carlson, B.; Fifield, L.; Phelan, G.; Kincaid, C.; Amend, J.; Jen, A. *J. Mater. Chem.* **1999**, *9*, 1905–1920.
(10) Wolff, J. J.; Wortmann, R. *Adv. Phys. Org. Chem.* **1999**, *32*, 121–217.
(11) Oudar, J. L.; Chemla, D. S. *J. Chem. Phys.* **1977**, *66*, 2664–2668.
(12) Oudar, J. L. *J. Chem. Phys.* **1977**, *67*, 446–457.
(13) Risser, S. M.; Beratan, D. N.; Marder, S. R. *J. Am. Chem. Soc.* **1993**, *115*, 7719–7728.
(14) Kanis, D. R.; Ratner, M. A.; Marks, T. J. *Chem. Rev.* **1994**, *94*, 195–242.
(15) Kanis, D. R.; Lacroix, P. G.; Ratner, M. A.; Marks, T. J. *J. Am. Chem. Soc.* **1994**, *116*, 10089–10102.
(16) Kuzyk, M. G. *Phys. Rev. Lett.* **2000**, *85*, 1218–1221.
(17) Kuzyk, M. G. *Phys. Rev. Lett.* **2005**, *95*, 053819.
(18) Hu, X.; Xiao, D.; Keinan, S.; Asselberghs, I.; Therien, M. J.; Clays, K.; Yang, W.; Beratan, D. N. *J. Phys. Chem. C* **2010**, *114*, 2349–2359.
(19) Meyers, F.; Marder, S. R.; Pierce, B. M.; Brédas, J. L. *J. Am. Chem. Soc.* **1994**, *116*, 10703–10714.
(20) Marder, S. R.; Cheng, L.-T.; Tiemann, B. G.; Friedli, A. C.; Blanchard-Desce, M.; Perry, J. W.; Skindhøj, J. *Science* **1994**, *263*, 511–514.
(21) LeCours, S. M.; Guan, H.-W.; DiMagno, S. G.; Wang, C. H.; Therien, M. J. *J. Am. Chem. Soc.* **1996**, *118*, 1497–1503.
(22) Priyadarshy, S.; Therien, M. J.; Beratan, D. N. *J. Am. Chem. Soc.* **1996**, *118*, 1504–1510.
(23) LeCours, S. M.; DiMagno, S. G.; Therien, M. J. *J. Am. Chem. Soc.* **1996**, *118*, 11854–11864.
(24) Karki, L.; Vance, F. W.; Hupp, J. T.; LeCours, S. M.; Therien, M. J. *J. Am. Chem. Soc.* **1998**, *120*, 2606–2611.
(25) Uyeda, H. T.; Zhao, Y.; Wostyn, K.; Asselberghs, I.; Clays, K.; Persoons, A.; Therien, M. J. *J. Am. Chem. Soc.* **2002**, *124*, 13806–13813.
(26) Kang, H.; Facchetti, A.; Zhu, P.; Jiang, H.; Yang, Y.; Cariati, E.; Righetto, S.; Ugo, R.; Zuccaccia, C.; Macchioni, A.; Stern, C. L.; Liu, Z.; Ho, S.-T.; Marks, T. J. *Angew. Chem., Int. Ed.* **2005**, *44*, 7922–7925.
(27) Zhang, T.-G.; Zhao, Y.; Asselberghs, I.; Persoons, A.; Clays, K.; Therien, M. J. *J. Am. Chem. Soc.* **2005**, *127*, 9710–9720.
(28) Zhang, T.-G.; Zhao, Y.; Song, K.; Asselberghs, I.; Persoons, A.; Clays, K.; Therien, M. J. *Inorg. Chem.* **2006**, *45*, 9703–9712.
(29) Xu, T.; Wu, S. P.; Miloradovic, I.; Therien, M. J.; Blasie, J. K. *Nano Lett.* **2006**, *6*, 2387–2394.
(30) Keinan, S.; Therien, M. J.; Beratan, D. N.; Yang, W. *J. Phys. Chem. A* **2008**, *112*, 12203–12207.
(31) Duncan, T. V.; Song, K.; Hung, S.-T.; Miloradovic, I.; Nayak, A.; Persoons, A.; Verbiest, T.; Therien, M. J.; Clays, K. *Angew. Chem., Int. Ed.* **2008**, *47*, 2978–2981.
(32) Reeve, J. E.; Collins, H. A.; De Mey, K.; Kohl, M. M.; Thorley, K. J.; Paulsen, O.; Clays, K.; Anderson, H. L. *J. Am. Chem. Soc.* **2009**, *131*, 2758–2759.
(33) Therien, M. J. *Nature* **2009**, *458*, 716–717.
(34) Lin, V. S.-Y.; DiMagno, S. G.; Therien, M. J. *Science* **1994**, *264*, 1105–1111.
(35) Lin, V. S.-Y.; Therien, M. J. *Chem.—Eur. J.* **1995**, *1*, 645–651.
(36) Shediac, R.; Gray, M. H. B.; Uyeda, H. T.; Johnson, R. C.; Hupp, J. T.; Angiolillo, P. J.; Therien, M. J. *J. Am. Chem. Soc.* **2000**, *122*, 7017–7033.
(37) Angiolillo, P. J.; Susumu, K.; Uyeda, H. T.; Lin, V. S.-Y.; Shediac, R.; Therien, M. J. *Synth. Met.* **2001**, *116*, 247–253.
(38) Susumu, K.; Therien, M. J. *J. Am. Chem. Soc.* **2002**, *124*, 8550–8552.
(39) Fletcher, J. T.; Therien, M. J. *Inorg. Chem.* **2002**, *41*, 331–341.
(40) Rubtsov, I. V.; Susumu, K.; Rubtsov, G. I.; Therien, M. J. *J. Am. Chem. Soc.* **2003**, *125*, 2687–2696.
(41) Susumu, K.; Duncan, T. V.; Therien, M. J. *J. Am. Chem. Soc.* **2005**, *127*, 5186–5195.
(42) Duncan, T. V.; Susumu, K.; Sinks, L. E.; Therien, M. J. *J. Am. Chem. Soc.* **2006**, *128*, 9000–9001.
(43) Duncan, T. V.; Wu, S. P.; Therien, M. J. *J. Am. Chem. Soc.* **2006**, *128*, 10423–10435.
(44) Screen, T. E. O.; Thorne, J. R. G.; Denning, R. G.; Bucknall, D. G.; Anderson, H. L. *J. Am. Chem. Soc.* **2002**, *124*, 9712–9713.
(45) Duncan, T. V.; Rubtsov, I. V.; Uyeda, H. T.; Therien, M. J. *J. Am. Chem. Soc.* **2004**, *126*, 9474–9475.
(46) Drobizhev, M.; Stepanenko, Y.; Dzenis, Y.; Karotki, A.; Rebane, A.; Taylor, P. N.; Anderson, H. L. *J. Phys. Chem. B* **2005**, *109*, 7223–7236.
(47) Strzalka, J.; Xu, T.; Tronin, A.; Wu, S. P.; Miloradovic, I.; Kuzmenko, I.; Gog, T.; Therien, M. J.; Blasie, J. K. *Nano Lett.* **2006**, *6*, 2395–2405.
(48) Duncan, T. V.; Ishizuka, T.; Therien, M. J. *J. Am. Chem. Soc.* **2007**, *129*, 9691–9703.
(49) Hisaki, I.; Hiroto, S.; Kim, K. S.; Noh, S. B.; Kim, D.; Shinokubo, H.; Osuka, A. *Angew. Chem., Int. Ed.* **2007**, *46*, 5125–5128.
(50) Thorley, K. J.; Hales, J. M.; Anderson, H. L.; Perry, J. W. *Angew. Chem., Int. Ed.* **2008**, *47*, 7095–7098.
(51) Zou, H.; Therien, M. J.; Blasie, J. K. *J. Phys. Chem. B* **2008**, *112*, 1350–1357.
(52) Fisher, J. A. N.; Susumu, K.; Therien, M. J.; Yodh, A. G. *J. Chem. Phys.* **2009**, *130*, 134506.
(53) Raymond, J. E.; Bhaskar, A.; Goodson, T., III; Makiuchi, N.; Ogawa, K.; Kobuke, Y. *J. Am. Chem. Soc.* **2008**, *130*, 17212–17213.
(54) Song, J.; Aratani, N.; Heo, J. H.; Kim, D.; Shinokubo, H.; Osuka, A. *J. Am. Chem. Soc.* **2010**, *132*, 11868–11869.
(55) Clays, K.; Wostyn, K.; Olbrechts, G.; Persoons, A.; Watanabe, A.; Nogi, K.; Duan, X.-M.; Okada, S.; Oikawa, H.; Nakanishi, H.; Vogel, H.; Beljonne, D.; Brédas, J.-L. *J. Opt. Soc. Am. B: Opt. Phys.* **2000**, *17*, 256–265.
(56) Ma, H.; Liu, S.; Luo, J.; Suresh, S.; Liu, L.; Kang, S. H.; Haller, M.; Sassa, T.; Dalton, L. R.; Jen, A. K.-Y. *Adv. Funct. Mater.* **2002**, *12*, 565–574.
(57) Dalton, L. R.; Harper, A. W.; Robinson, B. H. *Proc. Natl. Acad. Sci. U.S.A.* **1997**, *94*, 4842–4847.
(58) Robinson, B. H.; et al. *Chem. Phys.* **1999**, *245*, 35–50.
(59) Steier, W. H.; et al. *Chem. Phys.* **1999**, *245*, 487–506.
(60) Liakatas, I.; Cai, C.; Bösch, M.; Jäger, M.; Bosshard, C.; Günter, P.; Zhang, C.; Dalton, L. R. *Appl. Phys. Lett.* **2000**, *76*, 1368–1370.
(61) Dalton, L. *Adv. Polym. Sci.* **2002**, *158*, 1–86.
(62) Luo, J.; Haller, M.; Ma, H.; Liu, S.; Kim, T.-D.; Tian, Y.; Chen, B.; Jang, S.-H.; Dalton, L. R.; Jen, A. K.-Y. *J. Phys. Chem. B* **2004**, *108*, 8523–8530.
(63) Zyss, J. *Nonlinear Opt.* **1991**, *1*, 3–18.
(64) Brédas, J. L.; Meyers, F.; Pierce, B. M.; Zyss, J. *J. Am. Chem. Soc.* **1992**, *114*, 4928–4929.
(65) Zyss, J.; Dhenaut, C.; Chauvan, T.; Ledoux, I. *Chem. Phys. Lett.* **1993**, *206*, 409–414.
(66) Zyss, J.; Chau Van, T.; Dhenaut, C.; Ledoux, I. *Chem. Phys.* **1993**, *177*, 281–296.
(67) Verbiest, T.; Clays, K.; Samyn, C.; Wolff, J.; Reinhoudt, D.; Persoons, A. *J. Am. Chem. Soc.* **1994**, *116*, 9320–9323.
(68) Lambert, C.; Nöll, G.; Schmälzlin, E.; Meerholz, K.; Bräuchle, C. *Chem.—Eur. J.* **1998**, *4*, 2129–2135.
(69) McDonagh, A. M.; Humphrey, M. G.; Samoc, M.; Luther-Davies, B.; Houbrechts, S.; Wada, T.; Sasabe, H.; Persoons, A. *J. Am. Chem. Soc.* **1999**, *121*, 1405–1406.
(70) Wolff, J. J.; Siegler, F.; Matschiner, R.; Wortmann, R. *Angew. Chem., Int. Ed.* **2000**, *39*, 1436–1439.

(71) Le Bozec, H.; Le Bouder, T.; Maury, O.; Bondon, A.; Ledoux, I.; Deveau, S.; Zyss, J. *Adv. Mater.* **2001**, *13*, 1677–1681.
(72) Cho, B. R.; Park, S. B.; Lee, S. J.; Son, K. H.; Lee, S. H.; Lee, M.-J.; Yoo, J.; Lee, Y. K.; Lee, G. J.; Kang, T. I.; Cho, M.; Jeon, S.-J. *J. Am. Chem. Soc.* **2001**, *123*, 6421–6422.
(73) Hennrich, G.; Asselberghs, I.; Clays, K.; Persoons, A. *J. Org. Chem.* **2004**, *69*, 5077–5081.
(74) Le Floc'h, V.; Brasselet, S.; Zyss, J.; Cho, B. R.; Lee, S. H.; Jeon, S.-J.; Cho, M.; Min, K. S.; Suh, M. P. *Adv. Mater.* **2005**, *17*, 196–200.
(75) Maury, O.; Le Bozec, H. *Acc. Chem. Res.* **2005**, *38*, 691–704.
(76) Hennrich, G.; Omenat, A.; Asselberghs, I.; Foerier, S.; Clays, K.; Verbiest, T.; Serrano, J. L. *Angew. Chem., Int. Ed.* **2006**, *45*, 4203–4206.
(77) Kim, H. M.; Cho, B. R. *J. Mater. Chem.* **2009**, *19*, 7402–7409.
(78) Fiorini, C.; Charra, F.; Nunzi, J.-M.; Samuel, I. D. W.; Zyss, J. *Opt. Lett.* **1995**, *20*, 2469–2471.
(79) Nunzi, J.-M.; Charra, F.; Fiorini, C.; Zyss, J. *Chem. Phys. Lett.* **1994**, *219*, 349–354.
(80) Quintiliani, M.; Pérez-Moreno, J.; Asselberghs, I.; Vázquez, P.; Clays, K.; Torres, T. *J. Phys. Chem. B* **2010**, *114*, 6309–6315.
(81) Lin, V. S.-Y.; Iovine, P. M.; DiMagno, S. G.; Therien, M. J.; Malinak, S.; Coucouvanis, D. *Inorg. Synth.* **2002**, *33*, 55–61.
(82) Laha, J. K.; Dhanalekshmi, S.; Taniguchi, M.; Ambroise, A.; Lindsey, J. S. *Org. Process Res. Dev.* **2003**, 799–812.
(83) Sauer, J.; Heldmann, D. K.; Pabst, G. R. *Eur. J. Org. Chem.* **1999**, 313–321.
(84) Coe, B. J.; Thompson, D. W.; Culbertson, C. T.; Schoonover, J. R.; Meyer, T. J. *Inorg. Chem.* **1995**, 3385–3395.
(85) Constable, E. C.; Ward, M. D. *J. Chem. Soc., Dalton Trans.* **1990**, 1405–1409.
(86) Vogler, L. M.; Franco, C.; Jones, S. W.; Brewer, K. J. *Inorg. Chim. Acta* **1994**, *221*, 55–59.
(87) Kober, E. M.; Marshall, J. L.; Dressick, W. J.; Sullivan, B. P.; Caspar, J. V.; Meyer, T. J. *Inorg. Chem.* **1985**, *24*, 2755–2763.
(88) Adcock, P. A.; Keene, F. R.; Smythe, R. S.; Snow, M. R. *Inorg. Chem.* **1984**, 2336–2343.
(89) Papp, S.; Vanderkooi, J. M.; Owen, C. S.; Holtom, G. R.; Phillips, C. M. *Biophys. J.* **1990**, *58*, 177–186.
(90) Olbrechts, G.; Strobbe, R.; Clays, K.; Persoons, A. *Rev. Sci. Instrum.* **1998**, *69*, 2233–2241.
(91) Olbrechts, G.; Wostyn, K.; Clays, K.; Persoons, A. *Opt. Lett.* **1999**, *24*, 403–405.
(92) Heesink, G. J. T.; Ruiter, A. G. T.; van Hulst, N. F.; Bölger, B. *Phys. Rev. Lett.* **1993**, *71*, 999–1002.
(93) Kaatz, P.; Shelton, D. P. *J. Chem. Phys.* **1996**, *105*, 3918–3929.
(94) Heck, R. F. *Acc. Chem. Res.* **1979**, *12*, 146–151.
(95) Kumada, M. *Pure Appl. Chem.* **1980**, *52*, 669–679.
(96) Takahashi, S.; Kuroyama, Y.; Sonogashira, K.; Hagihara, N. *Synthesis* **1980**, 627–630.
(97) Negishi, E.; Luo, F.-T.; Frisbee, R.; Matsushita, H. *Heterocycles* **1982**, *18*, 117–122.
(98) Stille, J. K. *Angew. Chem., Int. Ed.* **1986**, *25*, 508–524.
(99) DiMagno, S. G.; Lin, V. S.-Y.; Therien, M. J. *J. Org. Chem.* **1993**, *58*, 5983–5993.
(100) DiMagno, S. G.; Lin, V. S.-Y.; Therien, M. J. *J. Am. Chem. Soc.* **1993**, *115*, 2513–2515.
(101) LeCours, S. M.; Phillips, C. M.; de Paula, J. C.; Therien, M. J. *J. Am. Chem. Soc.* **1997**, *119*, 12578–12589.
(102) For instance, the term "Q_x-state" is used to refer to the lowest-energy $\pi\pi^*$-derived transition that is polarized along the long-molecular axis in these RuPZn-based chromophores, but it is understood that MLCT ($d-\pi^*$) character is mixed with this *x*-polarized absorption.
(103) Angiolillo, P. J.; Lin, V. S.-Y.; Vanderkooi, J. M.; Therien, M. J. *J. Am. Chem. Soc.* **1995**, *117*, 12514–12527.
(104) Fletcher, J. T.; Therien, M. J. *J. Am. Chem. Soc.* **2002**, *124*, 4298–4311.
(105) Ostrowski, J. C.; Susumu, K.; Robinson, M. R.; Therien, M. J.; Bazan, G. C. *Adv. Mater.* **2003**, *15*, 1296–1300.
(106) Angiolillo, P. J.; Uyeda, H. T.; Duncan, T. V.; Therien, M. J. *J. Phys. Chem. B* **2004**, *108*, 11893–11903.
(107) Frail, P. R.; Susumu, K.; Huynh, M.; Fong, J.; Kikkawa, J. M.; Therien, M. J. *Chem. Mater.* **2007**, *19*, 6062–6064.
(108) McCusker, J. K. *Acc. Chem. Res.* **2003**, *36*, 876–887.
(109) Damrauer, N. H.; Weldon, B. T.; McCusker, J. K. *J. Phys. Chem. A* **1998**, *102*, 3382–3397.
(110) Damrauer, N. H.; Boussie, T. R.; Devenney, M.; McCusker, J. K. *J. Am. Chem. Soc.* **1997**, *119*, 8253–8268.
(111) Winkler, J. R.; Netzel, T. L.; Creutz, C.; Sutin, N. *J. Am. Chem. Soc.* **1987**, *109*, 2381–92.
(112) Kumble, R.; Palese, S.; Lin, V. S.-Y.; Therien, M. J.; Hochstrasser, R. M. *J. Am. Chem. Soc.* **1998**, *120*, 11489–11498.
(113) Jakubikova, E.; Chen, W.; Dattelbaum, D. M.; Rein, F. N.; Rocha, R. C.; Martin, R. L.; Batista, E. R. *Inorg. Chem.* **2009**, *48*, 10720–10725.
(114) Using the relation $-(\Delta G_{CS}) = E_{(0,0)} - E_{1/2}(D/D^+) + E_{1/2}(A^-/A)$, where $E_{(0,0)}$ is the excitation energy, and the $E_{1/2}(D/D^+)$ and $E_{1/2}(A^-/A)$ values were determined from cyclic voltammetric data (see Table 2), suggests that PZn-(4Ru) (**2**) features a diminished driving force for charge separation relative to chromophores **1** and **3**−**9**. Chromophore (estimated ΔG_{CS}): **1** (−0.79 V), **2** (−0.49 V), **3** (−0.76 V), **4** (−0.75 V), **5** (−0.59 V), **6** (−0.72 V), **7** (−0.68 V), **8** (−0.67 V). Note that these estimated driving forces are meant to provide qualitative insight only, given the strong electronic coupling in these supermolecular chromophores and the fact that the electronically excited states of these species do not separate a full unit of charge.
(115) Cyvin, S. J.; Rauch, J. E.; Decius, J. C. *J. Chem. Phys.* **1965**, *43*, 4083–4049.
(116) Bersohn, R.; Pao, Y.-H.; Frisch, H. L. *J. Chem. Phys.* **1966**, *45*, 3184–3198.
(117) Verbiest, T.; Clays, K.; Persoons, A.; Meyers, F.; Brédas, J.-L. *Opt. Lett.* **1993**, *18*, 525–527.
(118) An alternative convention in the NLO literature[31] assumes that from Kleinman conditions indices may be permutated, such that the value for the *xyz* component is identical for all 6 permutations. Note that this does not mean that the *xzy*, *yxz*, *yzx*, *zxy* and *zyx* components are zero and do not contribute; ref116 clearly indicates the necessity to sum over *i*, *j*, and *k* for $i \neq j \neq k$ to determine the β_{ijk} tensor components. This convention then leads to the expression $\beta_{HRS}{}^2 = [\langle\beta_{ZZZ}{}^2\rangle + \langle\beta_{YZZ}{}^2\rangle] = 120/35\ \beta_{xyz}{}^2$ for octopolar T_d, D_2, or D_{2d} symmetries. Note that this convention is also widely accepted, and results in an interpretation of the experimentally obtained $\beta_{HRS}{}^2$ values in terms of 6 nonzero β_{ijk} tensor components that are a factor of $6^{1/2}$ smaller in magnitude than that arrived at via the convention used in the compilation of the Table 4 data. As a case in point, a previously reported value of 440×10^{-30} esu for the β_{xyz} value of the compound $PZnE_2PZn$, derived according to the former convention,[31] transforms into 1080×10^{-30} esu when the β_{xyz} computational method of this paper is followed. It is important for the reader to appreciate that, whichever of these conventions are used for computing and reporting β_{xyz} values, the overall response for an octopolar NLO chromophore remains directly related to $\beta_{HRS}{}^2$, *the magnitude of which is unaffected* by the convention used to compute β_{xyz}.
(119) Clays, K.; Persoons, A. *Phys. Rev. Lett.* **1991**, *66*, 2980–2983.
(120) Dhenaut, C.; Ledoux, I.; Samuel, I. D. W.; Zyss, J.; Bourgault, M.; Le Bozec, H. *Nature* **1995**, *374*, 339–342.
(121) Morrison, I. D.; Denning, R. G.; Laidlaw, W. M.; Stammers, M. A. *Rev. Sci. Instrum.* **1996**, *67*, 1445–1453.
(122) Tretiak, S.; Mukamel, S. *Chem. Rev.* **2002**, *102*, 3171–3212.